Proceedings of the ASME 2015 34th International Conference on Ocean, Offshore and Arctic Engineering
OMAE2015
May 31-June 5, 2015, St. John's, Newfoundland, Canada

OMAE2015-41388

CONTROL OF AN OPEN-LOOP HYDRAULIC OFFSHORE WIND TURBINE USING A VARIABLE-AREA ORIFICE

Daniel Buhagiar
Dept. of Mechanical Engineering,
University of Malta,
Msida, Malta
daniel.buhagiar.08@um.edu.mt

Tonio Sant
Dept. of Mechanical Engineering,
University of Malta,
Msida, Malta

Marvin K. Bugeja
Dept. of Systems & Control Engineering,
University of Malta,
Msida, Malta

ABSTRACT

The viability of offshore wind turbines is presently affected by a number of technical issues pertaining to the gearbox and power electronic components. Current work is considering the possibility of replacing the generator, gearbox and electrical transmission with a hydraulic system. Efficiency of the hydraulic transmission is around 90% for the selected geometries, which is comparable to the 94% expected for conventional wind turbines. A rotor-driven pump pressurises seawater that is transmitted across a large pipeline to a centralised generator platform. Hydroelectric energy conversion takes place in Pelton turbine. However, unlike conventional hydro-energy plants, the head available at the nozzle entry is highly unsteady. Adequate active control at the nozzle is therefore crucial in maintaining a fixed line pressure and an optimum Pelton turbine operation at synchronous speed. This paper presents a novel control scheme that is based on the combination of proportional feedback control and feed forward compensation on a variable area nozzle. Transient domain simulation results are presented for a Pelton wheel supplied by sea water from an offshore wind turbine-driven pump across a 10 km pipeline.

NOMENCLATURE

A_N	nozzle area [m^2]
b_S	drivetrain damping constant [$Nmrad^{-1}s$]
$C_{(e)}$	elemental fluid capacitance [m^3Pa^{-1}]
C_d	viscous damping coefficient [-]
C_D	nozzle discharge coefficient [-]
$C_{f,k}$	constant friction torque coefficient [Nm^{-2}]
$C_{f,v}$	variable friction torque coefficient [s^{-1}]
C_p	rotor power coefficient [-]
C_s	volumetric loss (slip) coefficient [-]
D	rotor diameter [m]
D_p	pipeline internal diameter [m]
d_s	spear valve orifice diameter [m]
E_B	liquid bulk modulus [Pa]
e_p	pipeline internal surface roughness [m]
h_s	spear valve position [m]
$I_{(e)}$	elemental fluid inertia [kgm^{-4}]
J_P	pump rotational inertia [kgm^2]
J_R	rotor rotational inertia [kgm^2]
k_S	drivetrain stiffness constant [$Nmrad^{-1}$]
$L_{(e)}$	elemental pipeline length [m]
$M_{B,S}$	drivetrain bending moment [Nm]
M_P	pump torque [Nm]
M_R	rotor torque [Nm]
p_N	nozzle pressure [Pa]
p_P	pump pressure [Pa]
Q	flow rate [m^3s^{-1}]
$R_{(e)}$	elemental fluid resistance [$Pam^{-3}s$]
Re	Reynolds number [-]
U_{rot}	wind speed at rotor plane [ms^{-1}]
V_P	pump volumetric displacement [m^3rev^{-1}]
α_s	spear valve cone angle [˚]
β	pitch angle [˚]
ϕ_S	drivetrain torsional deflection [rad]
λ	tip speed ratio [-]
μ	liquid dynamic viscosity [$kgm^{-1}s^{-1}$]
ρ	liquid density [kgm^{-3}]
ρ_a	air density [kgm^{-3}]
θ_P	pump angular position [rad]
θ_R	rotor angular position [rad]

INTRODUCTION

Conventional offshore wind turbine designs are based on existing onshore technologies that are adapted to the open water environment. This incremental approach has led to a number of technical and economic issues that significantly hinder the viability of offshore wind. Forecasts based on existing technology indicate that offshore wind turbines will only make

up 10% of the total installed wind generation capacity in 2016 [1]. Moreover, conventional turbines are suited for depths not exceeding 30 m [2]. Much more vast and resourceful environments could be exploited through the use of floating turbines. By accessing deeper waters, the wind turbine would be away from coastal regions at sites were issues related to aesthetic, noise and ecological impacts are of a lesser concern.

Floating wind turbines using conventional generation methods, that is, using rotor-gearbox-generator assembly, are already in the prototyping stage. However, they will likely face the same technical issues as with conventional seabed-mounted turbines, although this time the stakes would be higher since maintenance and logistical costs have increased. Key issues have been identified to be the high rate of gearbox failure [3], the weight of the nacelle [4] and the presence of expensive high-maintenance electronics [5]. There is also a concern for the high dependency on copper, required for the generators and the large-scale power transmission system interconnecting the distant turbines to the electricity grid onshore [6].

Hydraulic Wind Turbines

One promising proposition for an offshore-specific solution is a shift to hydraulic transmission. With an improved power to weight ratio, and a lower requirement for nacelle-based hardware, wind turbines utilizing large scale hydraulic transmissions could be ideal for the offshore environment. One design concept being researched is the Delft Offshore Turbine (DOT) [4], which uses seawater-based hydraulics and a centralized generation concept. There are numerous publications on the modeling of different aspects of this hydraulic wind turbine. However, the focus has so far been on the wind turbine side, and although some work on the pipeline dynamics has been presented [7], there has been limited work on the hydro-mechanical conversion side of the system.

The use of open-loop seawater hydraulics is further promoted by the idea of utilizing the cold seawater to extract thermal energy from a district cooling system. This takes place by passing the water through a heat exchanger following the hydro-mechanical conversion stage. Previous work [8] has shown that the additional thermal component would compensate for any increased losses in the hydraulic circuit.

The aim of the present work is to assess the control requirements of a simplified hydraulic wind turbine using an open-loop seawater circuit. Modeling includes simplified rotor aerodynamics, the directly coupled digital displacement pump, a long pipeline and an orifice from which a fluid jet emanates and impinges onto the buckets of a synchronous Pelton turbine. A schematic is shown in . The focus is on controlling the velocity of the jet in order to optimize the behavior of the turbine. It is understood that in order to achieve optimum performance at a fixed Pelton wheel angular velocity, that is, at synchronous speed, the jet velocity must remain fixed [9]. The controller objective is therefore to maintain fixed jet velocity for a continuously varying flow rate. For a dynamic nozzle pressure, the fixed jet velocity condition translates to a fixed dynamic pressure drop across the nozzle.

Wind Turbine Control

Conventional variable speed wind turbines control consists of two principle regions of operation. As the turbine rotates in the region between the cut-in and rated wind speed, the objective is to optimize power extraction [10]. A method of torque control is utilized to maintain a fixed ratio between the rotor angular velocity and the wind speed, that is, a constant tip-speed ratio. This leads to optimized rotor aerodynamics and the maximum rate of kinetic energy extraction. Beyond the rated wind speed, the objective is to curtail power extraction by limiting rotor angular velocity to the rated value [10]. This protects the turbine and associated components. It is achieved by altering the pitch angle of the blades in order to limit the aerodynamic torque being generated by the wind.

In the present turbine design concept, the second region of control remains the same; a pitch controller is utilized to limit power beyond the rated condition. However, the first region of control typically utilizes the generator to limit torque. In this case, the generator is not present and torque control is achieved using a variable displacement pump coupled directly to the turbine shaft [4] [8]. By altering the displaced volume per revolution, the torque requirement of the pump can be adjusted and therefore used to optimize rotor aerodynamics in the first region of control.

In order to accurately simulate the wind turbine, two controllers are modeled, one for the pump displacement and another for the pitch control. Their operation is based on that of the NREL 5MW reference wind turbine [11], with some alterations to accommodate a directly driven pump instead of a gearbox and generator.

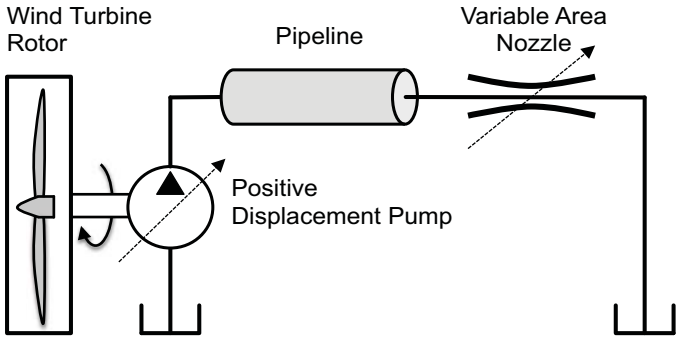

Figure 1: Simplified open-loop hydraulic circuit.

Pelton Turbine Control

Pelton turbines represent one of the most large-scale power conversion methods in the world; a single turbine can convert hundreds of megawatts of hydraulic energy [9]. In typical installations, the turbine is controlled using a variable-area orifice. This mechanism allows for adjusting the area of the nozzle that generates the jet that causes the Pelton wheel to rotate. Most large-scale systems operate at a fixed speed in conjunction with a grid-connected synchronous generator. Variable speed systems typically utilize alternative hydro-

mechanical converters such as Francis or Kaplan turbines [12], and they are not within the scope of the present work.

The aim of the variable area controller is to regulate to flow emanating from the nozzle, in conventional hydroelectric power plants, this depends on the power demand from the turbine. Given that these systems operate using a large reservoir, the head tends to remain nearly constant throughout turbine operation, such that the velocity of the fluid emerging from the nozzle is practically constant [9]. Essentially, conventional governing systems regulate flow rate in order to maintain synchronous speed. A fixed fluid velocity is maintained by the practically static-head at the reservoir, with some minor variations arising from dynamic losses in the penstock. A fixed fluid velocity and fixed Pelton turbine speed imply that the ratio between the two is also fixed; adequate sizing can give an optimum bucket-speed ratio that is maintained throughout the operation of the turbine. This ratio is crucial to optimizing the Pelton wheel efficiency. Theoretically, the optimum condition is when the bucket speed is around one-half of the jet speed. However, when considering windage losses in practical systems, the ideal ratio is around 0.48 [9].

There is a key difference between conventional hydroelectric generation and the system in the present study. The distinction is in the head at the nozzle: conventional systems utilize a primarily static head, whereas the proposed system utilizes a dynamic head. This is because the fluid is forced through the nozzle using a pump rather than a reservoir at a fixed elevation. The dynamic characteristics of the pump therefore have a significant impact on the fluid emanating from the nozzle. Moreover, the dynamic head depends on the flow rate. This is essentially the key difference and poses an additional challenge in developing an adequate nozzle controller. The system must cater for the variable flow rate being developed by the wind turbine-driven pump and alter the orifice area in order to maintain a fixed nozzle pressure and therefore optimum Pelton wheel operation at synchronous speed. This requirement is also briefly discussed by Laguna [7]. The aim of the present paper is to illustrate the development and simulation of such a controller within the proposed open-loop hydraulic turbine configuration. The variable-area orifice controller must satisfy the following objectives:

1. Maintain the desired fixed nozzle pressure over the operating range of wind speeds.
2. Adjust the area at a rate that is not fast enough to induce water hammer effects.

The second objective is important to avoid precarious system pressures arising from water hammering. This effect is caused by sudden changes in area that induce pressure waves across the pipeline. These waves can cause the pipeline to experience pressures several times the rated value [13]. Water hammering is typically avoided by imposing a speed limit on the motion of the spear valve [9]. However, this must not hinder the dynamic response of the control system and therefore a compromise needs to be reached.

SYSTEM MODEL

A transient model of the open-loop hydraulic wind turbine system () was developed in order to simulate the behavior of the control system. An overview of the model sub-components is presented; these include the rotor, drivetrain, positive displacement pump, pipeline and spear valve. The wind turbine-side controllers, that is, torque and pitch controllers, are also modeled since their behavior will affect the generated flow and corresponding pressure characteristics at the spear valve.

Wind Turbine Rotor

The selected rotor for the present system is that from the NREL 5MW reference wind turbine [11]. The model of the conversion of wind speed into mechanical power utilizes a look-up surface, shown in Figure 2, to obtain the power coefficient of the rotor. This parameter is defined as the ratio of extracted mechanical power to available wind power. Knowledge of the power coefficient (C_p) and the wind speed at the rotor (U_{rot}) allows for computing the extracted mechanical power. The power coefficient is itself dependent on the operating conditions of the rotor; these can be categorized as the rotor tip-speed ratio (λ) and pitch angle (β).

$$M_R\dot{\theta}_R = \frac{\frac{1}{8}\rho_a \pi D^2 {U_{rot}}^3}{C_p(\lambda,\beta)} \quad (1) \qquad \lambda = \frac{D\dot{\theta}_R}{2U_{rot}} \quad (2)$$

Simulations on the NREL 5MW reference wind turbine were carried out using FAST (Fatigue, Aerodynamics, Structures and Turbulence) with AeroDyn. These simulations are detailed in [11]. The steady-state response of the rotor can be obtained in the form of a look-up surface, as implemented in the FP7 project *Aeolus* [14].

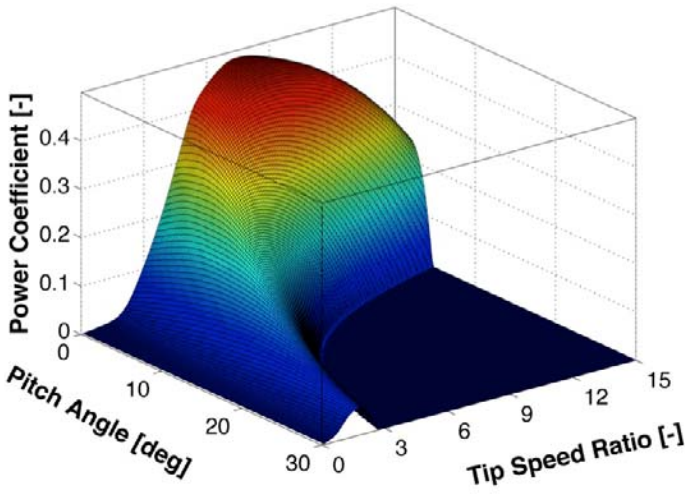

Figure 2: Power coefficient look-up surface.

Drive train

The drivetrain consists of a solid shaft connecting the rotor to the positive displacement pump. The properties of the mechanical transmission are based on those utilized by Jonkman et al. [11], although in this case there is no gearbox. Nonetheless, the stiffness and damping constants are taken to be identical. These give rise to a driveshaft natural frequency of around 0.62 Hz. The resulting damping ratio is 5% of the critical ratio. The inertia of the pump is extrapolated from the generator inertia of the NREL reference turbine [11], since there are no readily available values for pumps at this scale. The value was obtained by considering the fact that the pump would handle the torque of the NREL turbine generator multiplied by a factor of 97 (the gear-ratio of the NREL turbine drivetrain) since it would be directly connected to the rotor. This consideration led to reasoning that the pump's inertia would be 97 times that of the generator. Preliminary simulations confirm that system stability and frequency response are in fact maintained.

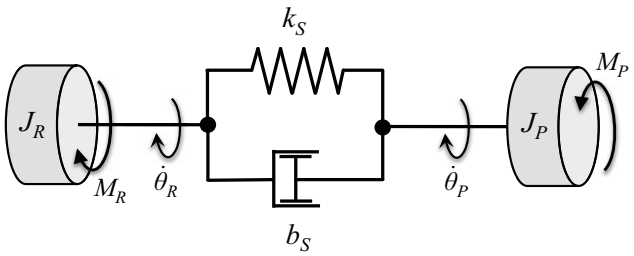

Figure 3: Free body diagram of the wind turbine drivetrain.

Considering the free body diagram of the drivetrain in Figure 3, the following state-space model of the drivetrain can be derived in terms of the inertias (J_R,J_P), damping (b_S) and stiffness (k_S).

$$\begin{bmatrix}\ddot{\theta}_R\\ \ddot{\theta}_P\\ \dot{\phi}_S\end{bmatrix} = \begin{bmatrix}-\frac{b_S}{J_R} & \frac{b_S}{J_R} & -\frac{k_S}{J_R}\\ \frac{b_S}{J_P} & -\frac{b_S}{J_P} & \frac{k_S}{J_P}\\ 1 & -1 & 0\end{bmatrix}\begin{bmatrix}\dot{\theta}_R\\ \dot{\theta}_P\\ \phi_S\end{bmatrix} + \begin{bmatrix}\frac{1}{J_R} & 0 & 0\\ 0 & -\frac{1}{J_P} & 0\\ 0 & 0 & 0\end{bmatrix}\begin{bmatrix}M_R\\ M_P\\ 0\end{bmatrix} \quad (3)$$

$$\begin{bmatrix}\dot{\theta}_R\\ \dot{\theta}_P\\ M_{B,S}\end{bmatrix} = \begin{bmatrix}1 & 0 & 0\\ 0 & 1 & 0\\ 0 & 0 & k_S\end{bmatrix}\begin{bmatrix}\dot{\theta}_R\\ \dot{\theta}_P\\ \phi_S\end{bmatrix}$$

In the above model, ϕ_S is the torsional deflection of the shaft, defined as the difference between the rotor and pump displacement. $M_{B,S}$ is the torsional bending moment on the driveshaft, defined below.

$$\phi_S = \theta_R - \theta_P \quad (4) \qquad M_{B,S} = k_S\phi_S \quad (5)$$

Hydraulic Pump

A generic lumped-parameter model of a positive displacement pump is described in this section. Such an approach allows for an efficient means of modeling the behavior of the positive-displacement pump as an energy conversion device, without modeling its internal dynamic behavior. This method has been used extensively in applications involving wind-turbine driven hydraulic pumps [4] [15]. It must be noted that this is a static model, since inertial and capacitive terms for the pump are not considered. In practice, these would correspond to the inertia of the fluid in the chamber and its compressibility, respectively. Kempenaar [16] carried out a dynamic analysis on a similar hydraulic transmission system and concluded that these parameters do not add any appreciable accuracy to the model. Such an assertion is particularly valid in this context, where the pump is connected to a very long pipeline and it can therefore be reasoned that the inertia and capacitance of the fluid in the pump chambers are negligible when compared those of the fluid in the pipeline.

Although the original model was derived for a traditional positive displacement pump, current work will focus on the use of Digital-Displacement® (DD) pumping. The main difference is that in DD, the pump chambers are activated or deactivated using electronic solenoid valves rather than the motion of a swash-plate. This allows for accurate and very fast control of the pump displacement. From a modeling perspective, the mechanical rather than volumetric efficiency is dependent on the current displacement of the pump. This is discussed by Silva et al. [17], who attribute this change in behavior to the fact that inactive pistons induce negligible volumetric losses, since their chamber pressure is approximately equal to the inlet pressure. On the other hand, the mechanical efficiency is affected since inactive pistons still induce frictional losses, and without contributing anything to the power conversion process, they inevitably reduce the efficiency. The pump torque (M_P) and flow rate (Q_P) are given in terms of the pressure load (p_P), viscosity (μ) and angular velocity ($\dot{\theta}_P$) of the pump:

$$M_P = V_{P,max}p_P\left[\frac{V_P}{V_{P,max}} + C_d\left(\frac{\mu\dot{\theta}_P}{p_P}\right) + C_{f,v}\left(\frac{1}{\dot{\theta}_P}\right) + C_{f,k}\left(\frac{1}{p_P}\right)\right] \quad (6)$$

$$Q_P = V_p\dot{\theta}_P\left[1 - C_s\left(\frac{p_P}{\mu\dot{\theta}_P}\right)\right] \quad (7)$$

The loss coefficients are shown in Table 1, they are obtained from a study by Silva et al. [17], for a multi-megawatt DD transmission coupled to a wind turbine rotor. A fundamental aspect of the lumped model technique is that these three terms are taken to remain constant throughout the operation of the pump [18]. V_p is the pump displacement.

Table 1: Loss coefficients of the pump model

Viscous Damping Coefficient [C_d]	24,064
Variable Friction Torque Coefficient [$C_{f,v}$]	0.0092 s^{-1}
Constant Friction Torque Coefficient [$C_{f,k}$]	118,000 Nm^{-2}
Volumetric Loss (Slip) Coefficient [C_s]	3.552×10^{-15}

Pipeline

The pipe flow dynamics are modelled using a second-order model that is analogous to a mass-spring-damper system. The dynamic elements of the pipeline are lumped into inertial, capacitive and resistive elements, as shown in Figure 4. Given known fluid properties and pipeline geometry, the individual terms can be computed using simple arithmetic relations, with the exception of the resistive term, which is where the complication arises [4]. The resistance encountered by a fluid flowing through a pipe is dependent on the flow rate, which is in turn dependent on the resistance it encounters [19]. Iterative methods are simple to use towards a steady-state solution, however the matter is further complicated in dynamic system modelling since the frictional effects are strongly linked to the current state of the model.

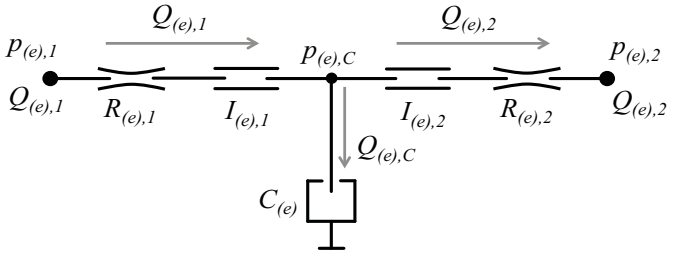

Figure 4: Fluid element of the NLTV pipeline model.

The proposed method tackles this issue by using a non-linear time-*variant* state-space model (NLTV), which is distinct from typically used linear time-invariant models (LTI). The main distinction is that the coefficient matrices in the state-space model are updated at every simulation step, specifically to reflect changes in the resistive terms. The model has four variables: the upstream flow and pressure ($Q_{(e),1}$, $p_{(e),1}$), and the downstream flow and pressure ($Q_{(e),2}$, $p_{(e),2}$). Two of these variables are known, and the remaining two can be computed from the state-space model that is given in terms of the elemental inertia ($I_{(e)}$), capacitance ($C_{(e)}$) and resistance ($R_{(e)}$):

$$\begin{bmatrix}\ddot{p}_{(e),C}\\ \dot{p}_{(e),C}\\ \dot{Q}_{(e),C}\end{bmatrix} = \begin{bmatrix}\frac{-2R_{(e),2}}{I_{(e)}} & \frac{-2}{I_{(e)}C_{(e)}} & 0\\ 0 & 0 & \frac{1}{C_{(e)}}\\ 0 & \frac{-2}{I_{(e)}} & \frac{-2R_{(e),2}}{I_{(e)}}\end{bmatrix}\begin{bmatrix}\dot{p}_{(e),C}\\ p_{(e),C}\\ Q_{(e),C}\end{bmatrix} + \begin{bmatrix}\frac{-2R_{(e),2}}{I_{(e)}C_{(e)}} & \frac{-2}{I_{(e)}C_{(e)}} & \frac{1}{C_{(e)}}\\ 0 & 0 & 0\\ \frac{-2R_{(e),2}}{I_{(e)}} & \frac{-2}{I_{(e)}} & 1\end{bmatrix}\begin{bmatrix}Q_{(e),1}\\ p_{(e),2}\\ \dot{Q}_{(e),1}\end{bmatrix} \quad \textbf{(8)}$$

$$\begin{bmatrix}Q_{(e),2}\\ p_{(e),1}\\ Q_{(e),C}\end{bmatrix} = \begin{bmatrix}0 & 0 & -1\\ 0 & 1 & 0\\ 0 & 0 & 1\end{bmatrix}\begin{bmatrix}\dot{p}_{(e),C}\\ p_{(e),C}\\ Q_{(e),C}\end{bmatrix} + \begin{bmatrix}1 & 0 & 0\\ R_{(e),1} & 0 & \frac{I_{(e)}}{2}\\ 0 & 0 & 0\end{bmatrix}\begin{bmatrix}Q_{(e),1}\\ p_{(e),2}\\ \dot{Q}_{(e),1}\end{bmatrix}$$

From basic definitions of fluid inertia, capacitance and resistance, the matrix coefficient terms can be defined. Equation **(11)** is the result of the Colebrook and White formula substituted into the Darcy-Weisbach equation [20].

$$I_{(e)} = \frac{4\rho L_{(e)}}{\pi {D_p}^2} \quad \textbf{(9)} \qquad C_{(e)} = \frac{\pi {D_p}^2 L_{(e)}}{4E_B} \quad \textbf{(10)}$$

$$R_{(e)} = \frac{8\rho L_{(e)} Q_{(e)}}{\pi^2 {D_p}^5}\left(-1.8\log\left[\frac{6.9}{\mathrm{Re}} + \left(\frac{e_p}{3.7D_p}\right)^{1.11}\right]\right)^{-2} \quad \textbf{(11)}$$

Of particular importance in the current study is the ability of the model to resolve the water hammer effect. A preliminary simulation using Simulink™ was carried out with a 0.3 m diameter, 1 km pipeline, a steady flow was applied and after around 30 s, the orifice area was quickly reduced to nearly zero. The area was increased to its original value after 125 seconds. Results are shown in Figure 5.

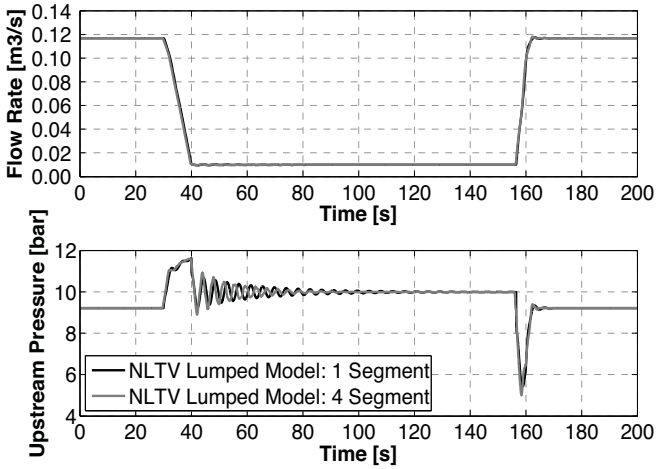

Figure 5: Water hammer effect simulated using one- and four-element NLTV models.

The two variants of the model predict a practically identical response in the flow rate. However, the single-element model slightly over-predicts the settling time for the pressure oscillations, there are also some minor discrepancies in the frequency decay. A positive attribute is that the less computationally demanding single-element model was able to compute an identical peak pressure to the four-element model.

Spear Valve

The hydraulic pressure is converted into kinetic energy using a variable-area nozzle. The dynamic pressure drop (p_N) at the nozzle is a function of the flow rate (Q), fluid density (ρ) nozzle area (A_N) and discharge coefficient (C_D) [20]:

$$p_N = \frac{1}{2}\rho\left(\frac{A_N}{C_D}\right)^2 Q^2 \quad \textbf{(12)}$$

A spear valve mechanism allows for continuously adjusting the effective area by shifting a tapered spear relative to a fixed circular orifice, this is illustrated in Figure 6. The effective area of the orifice (A_N) has the geometry of a frustum.

It is a function of the fixed orifice diameter (d_s), spear cone angle (α_s) and the variable spear position (h_s). The maximum effective area of the nozzle is the circular area corresponding to the orifice diameter, this occurs when the spear is fully retracted.

$$A_N(h_s) = \pi \left[h_s d_s \sin\left(\frac{\alpha_s}{2}\right) - {h_s}^2 \sin^2\left(\frac{\alpha_s}{2}\right) \cos\left(\frac{\alpha_s}{2}\right) \right] \quad (13)$$

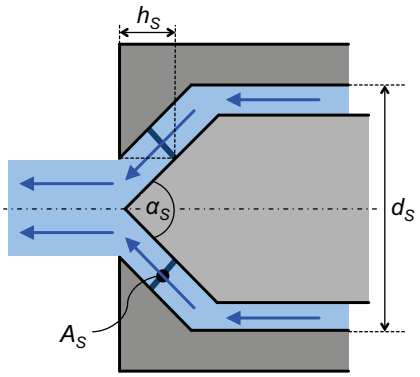

Figure 6: Simplified spear valve geometry.

The spear position is controlled using a linear servomotor. The motion occurs over relatively short strokes and the response is therefore very fast [21]. A speed limitation is typically imposed to limit water hammer effects [9]. The servomechanism is modeled as a second order system that receives the desired spear position from an external controller. Proportional Derivative (PD) feedback control is used to shift the spear into position. A block diagram is shown in Figure 7.

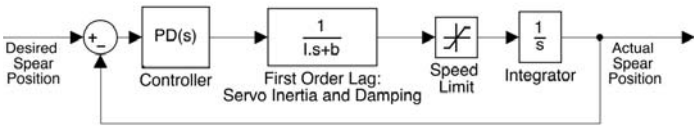

Figure 7: Spear valve servomechanism block diagram.

CONTROL SYSTEM DESIGN

In this section the main controllers are described, the open-loop hydraulic wind turbine uses three independent controllers to regulate and optimize its behavior.

1. Hydraulic torque control (Pump displacement controller)
2. Aerodynamic torque control (Pitch controller)
3. Pressure controller (Spear valve position)

The first two controllers are on the rotor-side of the system and a substantial amount of work has already been carried out on rotor control in both conventional and hydraulic wind turbines using variable displacement pumps [4] [15] [17]. The third controller is of main interest in the present work, as there is limited knowledge in this regard. This is crucial to the efficient operation of a fixed-speed Pelton turbine.

Rotor Control

In order to accurately model the system, and therefore the behavior of the pressure controller, the rotor controllers must be included. Given that their behavior is well understood, a brief description of their models is undertaken.

The hydraulic torque controller is responsible for adjusting the instantaneous displacement of the pump. The torque required to rotate the pump can therefore be set to the required value in order to ensure that the rotor is rotating at the optimum tip-speed ratio. In the present model, a simple feed-forward controller is implemented. Inverse pump dynamics are used to compute the required displacement from rotor speed and pressure sensor measurements. A block diagram of the pump controller is shown in Figure 8.

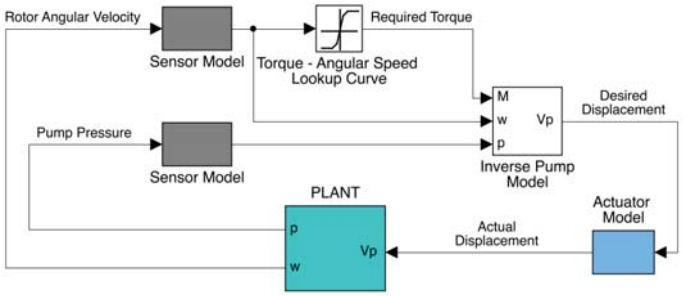

Figure 8: Pump controller block diagram.

The rotor speed measurement is converted into the required rotor torque using a look-up method as described by Jonkman et al. [11]. However, in the case of the conventional NREL 5MW wind turbine, the look-up curve was for rotor-gearbox-generator assembly. A new curve was generated by correcting the rotor torque and speed for the absence of the gearbox. It is reasonable to expect that the pump will have a torque requirement equivalent to a low speed generator [4].

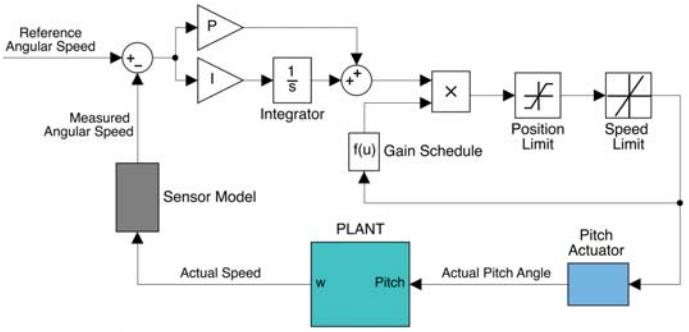

Figure 9: Pitch controller block diagram.

Hydraulic torque control is used between the cut-in and rated wind speeds, where rotor performance is optimized to maximize power harvesting. Beyond the rated wind speed, the pump displacement is set to its maximum and the pitch controller takes over. This was modeled as a gain-scheduled PI controller. A block diagram is shown in Figure 9. A more detailed description of the pitch controller can be found in [11].

Actuator and Sensor Modeling

In the previous section, reference is made to the pump displacement and pitch actuators; these consist of second-order systems that represent the time response of the actuator. Without actuator models, the controller behavior would be unrealistic since changes in the control variable would result in instantaneous changes in the output. In practice, it is understood there is a transient effect. In the case of the pitch controller, an oil circuit and hydraulic motor are used to shift the blade into position. The model takes into account the delay in the hydraulic piping and a first-order lag for the actuator transient response. A sensor model is also included in the feedback loop, this accounts for the sampling rate, resolution and transfer rate of the pitch position sensor. A block diagram is shown in Figure 10, numerical values are based on the model in [14].

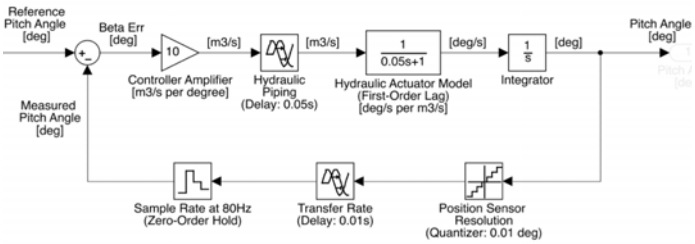

Figure 10: Pitch actuator block diagram.

A similar model is used for the pump displacement actuator, although in this case it models the time response of the solenoids in the digital displacement pump to activate. Its time response is expected to be very fast, since this is one of the advantages of DD pumping [17].

Where reference is made to a sensor model, this consists of the same components shown in the feedback loop of Figure 10. In the case of the angular speed sensor, a single-pole recursive low pass filter is used to eliminate any high frequency oscillations that give numerical problems. The corner frequency was set to 0.25 Hz. The use of the filter is discussed by Jonkman et al. [11] and implemented by Grunnet et al. [14].

Pressure Controller

The dynamic nozzle pressure is controlled using the spear valve. This control system must maintain a fixed pressure drop across the nozzle for a sporadically changing flow rate. The flow generated by the pump depends in the wind speed. By fixing the nozzle pressure, the jet velocity remains fixed, therefore allowing for optimized performance of the Pelton turbine at synchronous speed. Moreover, a fixed nozzle pressure implies stable and controlled pipeline dynamics, and consistent operation of an adequately sized pump.

Given the non-linear nature of the variable area orifice, a simple PID feedback controller is not enough to regulate the pressure. The first attempt at a pressure controller consists of a Feed Forward Control (FFC) concept that utilizes a model of the orifice and spear valve as a compensator. Equations (12) and (13) give the relationship between spear valve position and the nozzle pressure at a particular flow rate.

$$K_1 {h_s}^4 + K_2 {h_s}^3 + K_3 {h_s}^2 - \frac{p_N^*}{Q^2} = 0 \qquad \textbf{(14)}$$

In the above relation, K_1, K_2, and K_3 are constants that can be computed from the fixed parameters of the orifice and spear valve; p_N^* is the desired nozzle pressure. Solving the quartic equation (14) for h_s gives the spear valve position required to maintain the desired nozzle pressure. Of course there are four solutions for each set (p_N^*, Q), however only one solution falls within the practical range of spear valve positions. A block diagram of the original feed forward concept is shown in Figure 11.

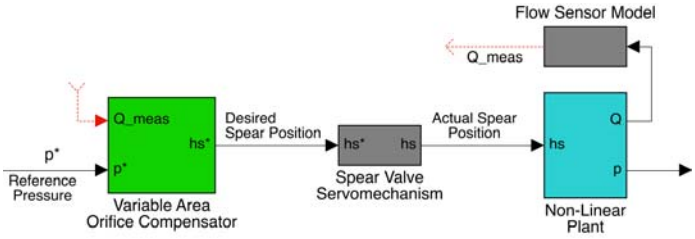

Figure 11: Feed forward controller block diagram.

The main drawback of the FFC is that it is highly dependent on the accuracy of the model it uses as a compensator. In order to observe this behavior in the present context a sensitivity analysis was undertaken. Parameters were adjusted in the simulated model without making the same adjustments in the compensator. These variations correspond to practical deviations from modeled behavior. The study consisted of altering the nozzle diameter and observing changes in the steady-state pressure maintained by the controller.

Sensitivity analysis results for the FFC are shown in Figure 12. It can easily be observed that minor variations in the physical system parameters lead to substantial deviations in the steady-state behavior of the controller. A change in the orifice characteristics of just 5% is enough to cause a 10% steady-state error due to the nonlinear relation between the spear-valve position and pressure along with the lack of robustness of the FFC scheme. This is a serious flaw of the controller, since it is expected that with practical use, the physical system will experience deviations from theoretical behavior due to fouling, corrosion and temperature effects.

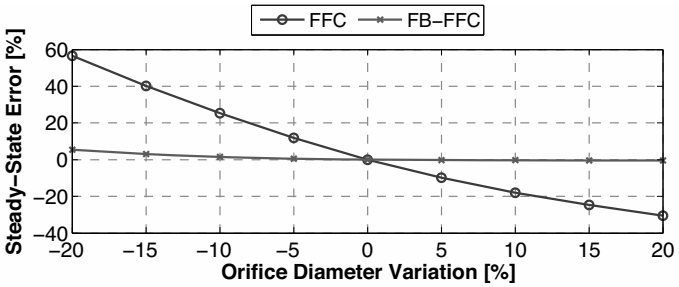

Figure 12: Controller sensitivity analysis.

An improvement on the original controller was to include an additional feedback loop (Figure 13). Through directly measuring the pressure across the orifice in conjunction with the flow rate, the orifice controller can use the compensator for the nonlinear part of the system and the feedback loop for trimming the pressure to the required value. This concept is referred to as feedback with feed forward compensation (FB-FFC) [22] and has been used in non-linear control of mechanical actuators similar to the present application [23].

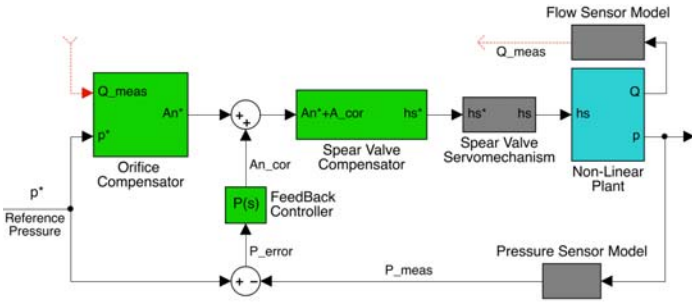

Figure 13: FB-FFC controller block diagram.

The hybrid controller is much more robust in the face of uncertain dynamics, as can be seen from the sensitivity analysis. Figure 12 shows how drastic variations between the compensator model and physical system only give rise to minimal deviations in the steady-state value.

SIMULATION RESULTS

In this section, the objective of the simulations was to obtain performance characteristics of the open-loop hydraulic circuit. The primary focus was the spear valve controller and its effect on the dynamic characteristics of the system. The models were fed artificial wind data and the simulation was started at the steady-state pressure. The wind data was selected to have an average wind speed of 10 ms^{-1}, close to the rated speed of the turbine, and a high turbulence intensity of 20%. It was generated using a von Karman energy spectrum, as utilized in similar work [7] [14]. Other simulation parameters are shown in Table 2.

Table 2: Simulation Parameters

Spear Valve Orifice Diameter	0.07 m
Spear Valve Cone Angle	90˚
Pipeline Internal Diameter	0.5 m
Pipeline Length	10 km
Pump Maximum Displacement	1.75 m^3rev^{-1}
Rated Nozzle Pressure	150 bar

The overall response was drastically improved with the FB-FFC concept, as can be observed in Figure 14. It can be observed that the FFC alone is able to maintain an adequate steady-state value with deviations in the order of ± 2 bar. However, in this simulation the compensator parameters are set to perfectly match those of the physical system model. The FB-FCC controller maintains the line pressure to within ± 0.005 bar, and is much better at handling variations between predicted and actual system behavior. This is due to the real-time feedback that increases sensitivity to the system dynamics.

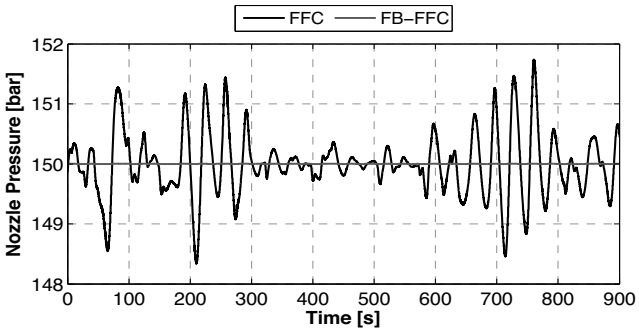

Figure 14: Pressure response of the FFC and FB-FFC controllers.

Transient simulation results are shown in Figure 15, where this time the line pressure was started at zero gauge pressure. The wind data fed into the model is shown in graph (a). All simulations were carried out within the MATLAB-Simulink™ environment. Rotor angular velocity is shown in graph (b), were it can be observed that minimal torsional deflection is predicted by the drivetrain model, since the rotor and pump velocity are nearly identical. The angular velocities are maintained at the rated value when the wind speed exceeds the rated value of 11.4 ms^{-1}. This highlights adequate displacement and pitch controller performance. Graph (c) shows the rotor and pump torque. The drivetrain is absorbing a number of torque fluctuations, particularly at the rated wind speed. Pump displacement and pitch angle are shown in graph (d). The pump displacement sharply increases from zero to the maximum value as the rotor accelerates. It then tracks the wind speed by increasing torque loading as the rotor accelerates in order to maintain the optimum tip-speed ratio. Beyond the rated wind speed, the pitch controller limits the angular velocity.

Hydraulic pressures are shown in graph (e), as soon as the line pressure is established at the nozzle, the FB-FCC controller is able to maintain this value throughout the simulation. The pump pressure on the other hand experiences some fluctuations that are mainly related to the non-linear pipeline dynamics, which result in fluctuations related to the flow-rate. The pump and nozzle flows are shown in graph (f), the pipeline dynamics and spear valve motion imply a significant variation between the two, particularly in the initial transient response. At the steady-state pressure, there are a number of fluctuations at the pump-side that are mainly dependent on the wind speed. At the nozzle-side fluctuations are caused by the pipeline dynamics and the spear valve motion. Graph (g) shows the spear valve position, which is strongly correlated with the flow rate, as this parameter changes, the spear must move in order to maintain the nozzle pressure.

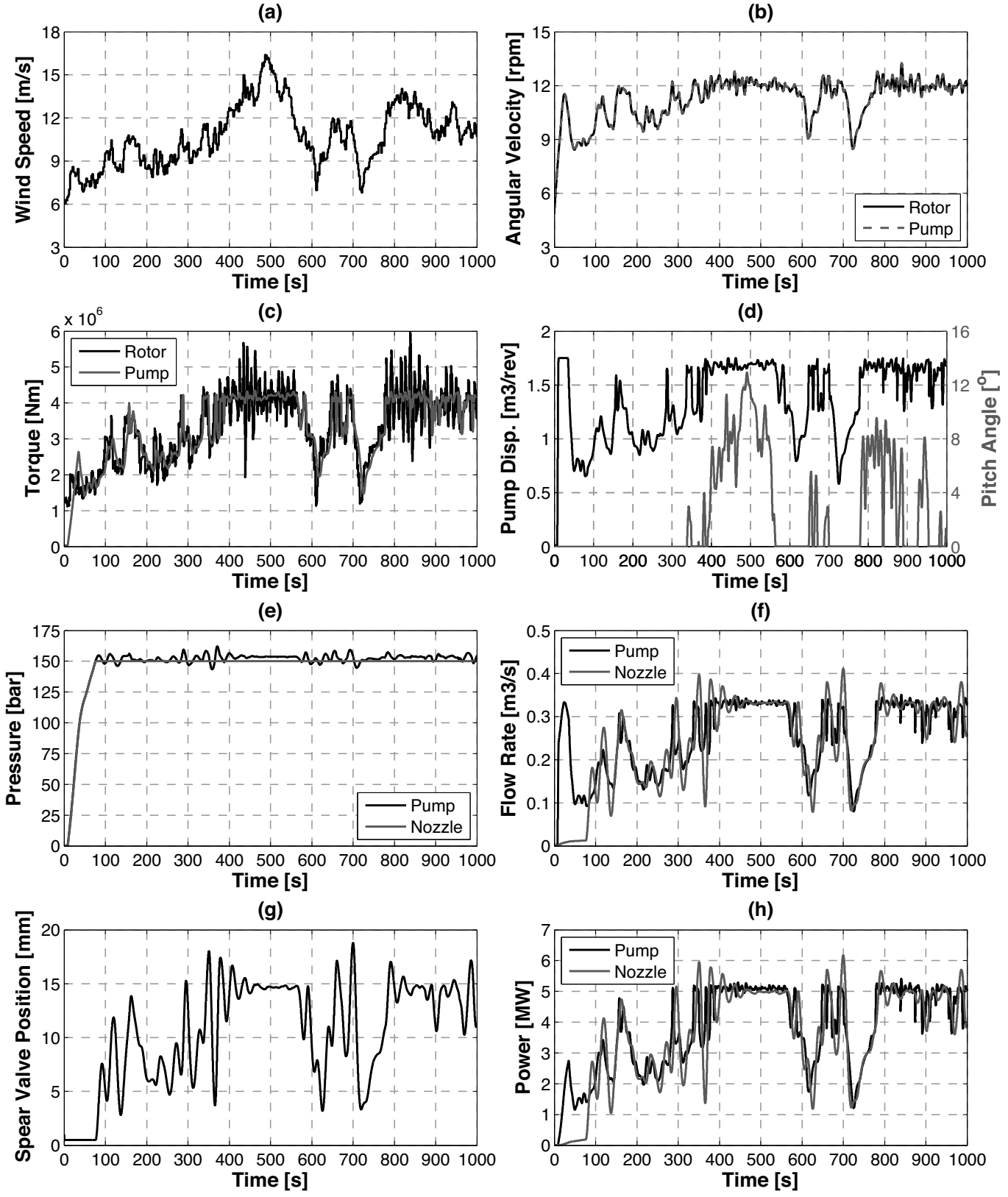

Figure 15: Simulation results for the open-loop system using the FB-FCC controller.

The precise tracking results in a stable nozzle pressure, however it also results in significant flow fluctuations. These translate to wide transients in the output power, as shown in Graph (h). The power is directly related to the flow and it might therefore be worth considering flow fluctuations in the controller design. Significant differences in flow, particularly in the initial transient response, are due to the compressibility of the relatively large volume of fluid within the pipeline.

CONCLUSION

A simulation model for the conceptual open-loop hydraulic wind turbine has been presented. A controller using a combination of feed forward compensation and feedback was shown to be an ideal candidate for dynamic pressure regulation. Simulation results indicate adequate system behavior under a range of wind speeds.

Of particular note is the occurrence of wide power fluctuations at the nozzle. Despite a fixed line pressure, the flow experiences significant transients, which might affect the output power from the turbine. On the other hand, the present model does not account for the hydro-electrical conversion process. Given the fixed nozzle pressure, it is to be expected that the Pelton turbine can operate at a fixed synchronous speed and that the hydro-mechanical conversion process is continuously optimized. It can therefore be reasoned that sharp flow fluctuations are absorbed by the favorable inertia of the Pelton turbine. This is the scope of future work, where a dynamic model of the Pelton wheel will be interfaced with the present model. Other schemes of control for the spear valve can also be considered, giving rise to less flow variations at the expense of wider pressure fluctuations that are still acceptable.

Also within the scope of future work is the possibility of including an energy storage system between the pump and nozzle. This will contribute to the minimization of flow fluctuations and allow for a more consistent power output from the system.

ACKNOWLEDGMENT

The research work disclosed in this publication is partly funded by the Malta Government Scholarship Scheme.

REFERENCES

[1] Global Wind Energy Council, "Global Wind Statistics 2013," Statistical Report 2014.

[2] A. Garran Hassan (Henderson, M. Gleeson, U. Kaufmes, J. Jacquemin, and C.) Morgan, "Offshore Wind Due Diligence," in *European Offshore Wind Conference*.

[3] Adam M. Ragheb and Magdi Ragheb, "Wind Turbine Gearbox Technologie," *Fundamentals and Advanced Topics in Wind Power*, pp. 189-206, July 2011.

[4] N. Diepeveen, "On the Application of Fluid Power Transmission in Offshore Wind Turbines," Delft University of Technology, Ph.D. Thesis 2013.

[5] S. Sheng, "Investigation of Various Wind Turbine Drivetrain Condition Monitoring Techniques," in *Wind Turbine Reliability Workshop*, USA, 2011, NREL/PR-5000-52352.

[6] R Ackerman, "A Bottom In Sight For Copper," *Forbes*, 2009.

[7] A.J. Laguna, "Fluid power network for centralized electricity generation in offshore wind farms ," in *Journal of Physics: Conference Series - The Science of Making Torque from Wind*, vol. 524, Copenhagen, 2014, doi:10.1088/1742-6596/524/1/012075.

[8] D. Buhagiar and T. Sant, "Steady-state analysis of a conceptual offshore wind turbine driven electricity and thermocline energy extraction plant," *Renewable Energy*, vol. 68, pp. 853-867, April 2014.

[9] S. L. Dixon, *Fluid Mechanics and Thermodynamics of Turbomachinery*, 5th ed. Oxford, United Kingdom: Elsevier Butterworth-Heinemann, 1998.

[10] J. Manwell, J. McGowan, and A. Rogers, *Wind Energy Explained, Theory, Design and Application*. England: John Wiley & Sons, 2002.

[11] J. Jonkman, S. Butterfield, W. Musial, and G. Scott, "Definition of a 5-MW Reference Wind Turbine for Offshore System Development," U.S. Department of Energy, National Renewable Energy Laboratory, Golden, CO, Technical Report 2009.

[12] J. Fraile-Ardanuy, J. R. Wilhelmi, J. J. Fraile-Mora, and J. I. Perez, "Variable-Speed Hydro Generation: Operational Aspects and Control," *IEEE Transactions on Energy Conversion*, vol. 21, no. 2, pp. 569-574, June 2006.

[13] B. E. Larock, R. W. Jeppson, and G. Z. Watters, *Hydraulics of Pipeline Systems*. USA: CRC Press, 1999.

[14] J. D. Grunnet, M. Soltani, T. Knudsen, M. Kragelund, and T. Bak, "Aeolus Toolbox for Dynamics Wind Farm Model, Simulation and Control," in *The European Wind Energy Conference & Exhibition, EWEC*, Warszawa, 2010.

[15] Antonio Jarquin Laguna, "Steady-State Performance of the Delft Offshore Turbine," Faculty of Aerospace Engineering, Delft University of Technology, Delft, M.Sc. Thesis 2010.

[16] A. Kempenaar, "Small Scale Fluid Power Transmission for the Delft Offshore Turbine," Faculty of Applied Physics, Delft University of Technology, M.Sc. Thesis 2012.

[17] P. Silva et al., "Performance prediction of a multi-MW wind turbine adopting an advanced hydrostatic transmission," *Energy*, vol. 64, no. 1, pp. 450-461, January 2014.

[18] H.E. Merritt, *Hydraulic Control Systems*.: John Wiley & Sons., Inc., 1967.

[19] Frank M. White, *Viscous Fluid Flow*.: McGraw-Hill, 1991.

[20] Frank M. White, *Fluid Mechanics*, 4th ed. Rhode Island, USA: McGraw Hill, 1998.

[21] A. Pisano and E. Usai, "Output-feedback control of an underwater vehicle prototype by higher-order sliding modes," *Automatica*, vol. 40, pp. 1525-1531, March 2004.

[22] R. Isermann, "Information processing for mechatronic systems," *Robotics and Autonomous Systems*, vol. 19, no. 2, pp. 117-134, December 1996.

[23] R. Grepl and B. Lee, "Modeling, parameter estimation and nonlinear control of automotive electronic throttle using a Rapid-Control Prototyping technique," *International Journal of Automotive Technology*, vol. 11, no. 4, pp. 601-610, August 2010.